Chaotic Modeling and Simulation (2011) : -

Symmetry-Breaking of Interfacial Polygonal Patterns and Synchronization of Travelling Waves within a Hollow-Core Vortex

Amr Mandour, Mohamed Fayed, Hamid Ait Abderrahmane, Hoi Dick Ng[1], Lyes Kadem and Georgios H. Vatistas

[1] Concordia University, Montréal, QC, H3G 1M8, Canada
(E-mail: hoing@encs.concordia.ca)

Abstract: A hollow vortex core in shallow liquid, produced inside a cylindrical reservoir using a rotating disk near the bottom of the container, exhibits interfacial polygonal patterns. These pattern formations are to some extent similar to those observed in various geophysical, astrophysical and industrial flows. In this study, the dynamics of rotating waves and polygonal patterns of symmetry-breaking generated in a laboratory model by rotating a flat disc near the bottom of a cylindrical tank is investigated experimentally. The goal of this paper is to describe in detail and to confirm previous conjecture on the generality of the transition process between polygonal patterns of the hollow vortex core under shallow water conditions. Based on the image processing and an analytical approach using power spectral analysis, we generalize in this work – using systematically different initial conditions of the working fluids – that the transition from any *N-gon* to *(N+1)-gon* pattern observed within a hollow core vortex of shallow rotating flows occurs in an universal two-step route: a quasi-periodic phase followed by frequency locking (synchronization). The present results also demonstrate, for the first time, that all possible experimentally observed transitions from *N*-gon into (*N*+1)-gon occur when the frequencies corresponding to *N* and *N*+1 waves lock at a ratio of (*N*-1)/*N*.
Keywords: Swirling flow, patterns, transition, quasi-periodic, synchronization.

1 Introduction

Swirling flows produced in closed or open stationary cylindrical containers are of fundamental interest; they are considered as laboratory model for swirling flows encountered in nature and industries. These laboratory flows exhibit patterns which resemble to a large extent the ones observed in geophysical, astrophysical and industrial flows. In general, the dynamics and the stability of such class of fluid motion involve a solid body rotation and a shear layer flow. Because of the cylindrical confining wall, the shear layer flow forms the outer region while the inner region is a solid body rotation flow. The interface between the flow regimes can undergo Kelvin-Helmholtz instability because of the jump in velocity at the interface between the inner and outer regions, which manifests as azimuthal waves. These waves roll up into satellite vortices which impart the interface polygonal shape, e.g., see [5, 9, 11-13]. The inner solid body rotation region can also be subjected to inertial instabilities which manifest

Received: 2011 / Accepted

as Kelvin's waves and it is this type of waves that will be investigated in this paper. In our experiment a hollow core vortex, produced by a rotating disk near the bottom of a vertical stationary cylinder, is within the inner solid body rotation flow region and acts as a wave guide to azimuthal rotating Kelvin's waves. The shape of the hollow core vortex was circular before it breaks into azimuthal rotating waves (polygonal patterns) when some critical condition was reached.

A fundamental issue that many research studies were devoted to the study of rotating waves phenomena is the identification and characterization of the transition from symmetrical to non-symmetrical swirling flows within cylindrical containers. Whether confined or free surface flow, the general conclusion from all studies confirmed that, the Reynolds number and aspect ratio (water initial height H / cylinder container radius R) are generally the two dominant parameters influencing the symmetry breaking phenomenon's behavior. Escudier [7] and Vogel [16] studied the transitional process in confined flows and found that symmetry breaking occurs when a critical Reynolds number was reached for each different aspect ratio. Vogel [16] used water as the working fluids in his study where he observed and defined a stability range, in terms of aspect ratio and Reynolds number, for the vortex breakdown phenomenon which occurred in the form of a moving bubble along the container's axis of symmetry. Escudier [7] later extended the study by using an aqueous glycerol mixture (3 to 6 times the viscosity of water) and found that varying the working fluid viscosity caused changes in the critical Reynolds number values. He also observed that for a certain range of aspect ratio and viscosity, the phenomenon of vorticity breakdown has changed in behavior, revealing more vortices breakdown stability regions than the conventional experiments using water as the working fluid. Where in open free surface containers under shallow liquid conditions using water as the working fluid, Vatistas [14] studied the transitional flow visually and found that the range of the disc's RPM where the transitional process occurs shrinks as the mode shapes number increased. Jansson et al. [10] concluded that the end-wall shear layers as well as the minute wobbling of the rotating disc are the main two parameters influencing the symmetry breaking phenomenon and the appearance of the polygonal patterns. Vatistas et al. [15] studied the transition between polygonal patterns from N to $N+1$, using image processing techniques, with water as the working fluid and found that the transition process from N to a higher mode shape of $N+1$ occurs when their frequencies ratio locks at $(N-1)/N$, therefore following a devil staircase scenario which also explains the fact that the transition process occurs within a shorter frequency range as the mode shapes increase. Speculating the transition process as being a bi-periodic state, the only way for such system to lose its stability is through frequency locking [4]. From nonlinear dynamics consideration, Ait Abderrahmane et al. [2] proposed the transition between equilibrium states under similar configurations using classical nonlinear dynamic theory approach and found that the transition occurs in two steps being, a quasi-periodic and frequency locking stages, i.e., the transition occurs through synchronization of the quasi-periodic regime formed

by the co-existence of two rotating waves with wave numbers *N* and *N+1*. Their studies however was built mainly on the observation of one transition, from *3-gon* to *4-gon*.

In the present paper, we provide further details on the symmetry-breaking pattern transitions and confirm the generalized mechanism on the transition from *N-gon* into *(N+1)-gon* using power spectra analysis. This study systematically investigates different mode transitions, the effect of working fluid with varying viscosity, liquid initial height on the polygonal pattern instability observed within the hollow core.

2 Experimental Setup and Measurement Technique

The experiments were conducted in a 284 mm diameter stationary cylindrical container with free surface (see Figure 1). A disk, located at 20 mm from the bottom of the container, with radius R_d = 126 mm was used and experiments with three initial water heights above the disk, h_o = *20, 30* and h_o = *40 mm*, were conducted. Similar experiment was conducted by Jansson et al. [10] within a container of different size where the distance of the disk from the bottom of the container is also much higher than in the case of our experiment. In both experiments similar phenomenon – formation of a polygonal pattern at the surface of the disk – was observed. It appears therefore that the dimension of the container and the distance between the disk and the container bottom do not affect the mechanism leading to the formation of the polygon patterns. In our experiment, the disk was covered with a thin smooth layer of white plastic sheet. It is worth noting that the roughness of the disk affects the contact angle between the disk and the fluid; this can delay the formation of the pattern. However, from our earlier observation in many experiments, roughness of the disk does not seem to influence prominently the transition mechanism.

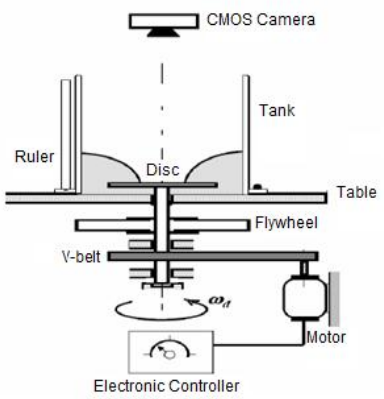

Fig. 1. Experimental setup.

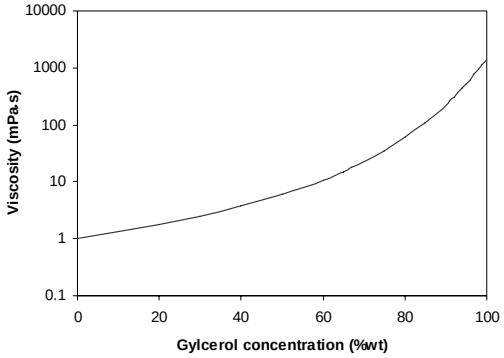

Fig. 2. The variation of dynamic viscosity as a function of glycerol concentration (by weight %wt).

The disk speed, liquid initial height and viscosity were the control parameters in this study. The motor speed, therefore the disc's speed, was controlled using a PID controller loop implemented on LABVIEW environment. Experiments with tape water and aqueous glycerol mixtures, as the working fluids, were conducted at three different initial liquid heights of 20, 30 and 40 mm above the rotating disc. The viscosity values of the used mixtures were obtained through technical data provided by a registered chemical company - Dow Chemical Company 1995-2010 [6]. Eight different aqueous glycerol mixtures were used in the experiments with viscosity varying from 1 to 22 (0 ~ 75% glycerol) times the water's at room temperature (21°C). The detailed points of study were: 1, 2, 4, 6, 8, 11, 15 and 22 times the water's viscosity (μ_{water}) at room temperature. Although the viscosity of the mixture varied exponentially with the glycerol concentration (see Figure 2), closer points of study were conducted at low concentration ratios since significant effects have been recognized by just doubling the viscosity of water as it will be discussed later. The temperature variation of the working fluid was measured using a mercury glass thermometer and recorded before and just after typical experimental runs and was found to be stable and constant (i.e. room temperature). Therefore, the viscosity of the mixture was ensured to be constant and stable during the experiment. Phase diagrams had been conducted and showed great approximation in defining the different regions for existing patterns in terms of disc's speed and initial height within the studied viscosity range.

A digital CMOS high-speed camera (pco.1200hs) with a resolution of 1280 x 1024 pixels was placed vertically above the cylinder using a tripod. Two types of images were captured: colored and 8-bit gray scale images, at 30 frames per second, for the top view of the formed polygonal patterns (see Figure 3 for example). The colored images were used as illustration of the observed stratification of the hollow vortex core where each colored layer indicates a water depth within the vortex core. It is worth noticing that the water depth increases continuously as we move away from the center of the disk (due to the

applied centrifugal force). The continuous increase in the water depth, depicted in the Figure 3 by the colored layers, indicates momentum stratification in the radial direction (i.e., starting with the central white region which corresponds to a fully dry spot of the core and going gradually through different water depth phases until reaching the black color region right outside the polygonal pattern boundary layer). For subsequent quantitative analysis, the data was conducted with grey images as those are simpler for post-processing.

The transition mechanism is investigated using image processing techniques. First the images were segmented; the original 8-bit gray-scale image is converted into a binary image, using a suitable threshold, to extract the polygonal contours [8]. This threshold value is applied to all subsequent images in a given run. In the image segmentation process, all the pixels with gray-scale values higher than the threshold were assigned 1's (i.e., bright portions) and the pixels with gray-scale values lower than or equal to the threshold were assigned 0's (i.e., dark portions). The binary image obtained after segmentation is filtered using a low-pass Gaussian filter to get rid of associated noises. In the next step, the boundaries of the pattern were extracted using the standard edge detection procedure. The pattern contours obtained from the edge detection procedure were then filtered using a zero-phase filter to ensure that the contours have no phase distortion. The transformations of the vortex core are analyzed using Fast Fourier Transform (FFT) of the time series of the radial displacement for a given point on the extracted contour, defined by its radius and its angle in polar coordinates with origin at the centroid of the pattern; see [1-3] for further details.

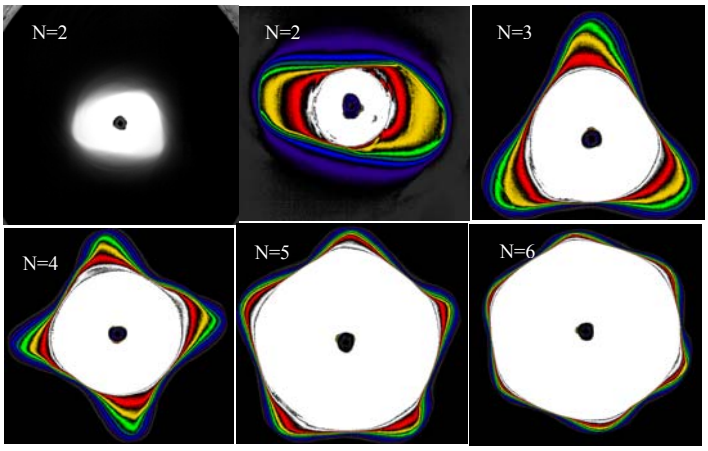

Fig. 3. Polygonal vortex core patterns. The inner white region is the dry part of the disk and the dark spot in the middle of the image is the bolt that fixes the disk to the shaft. The layers with different colors indicate the variation of water depth from the inner to the outer flow region.

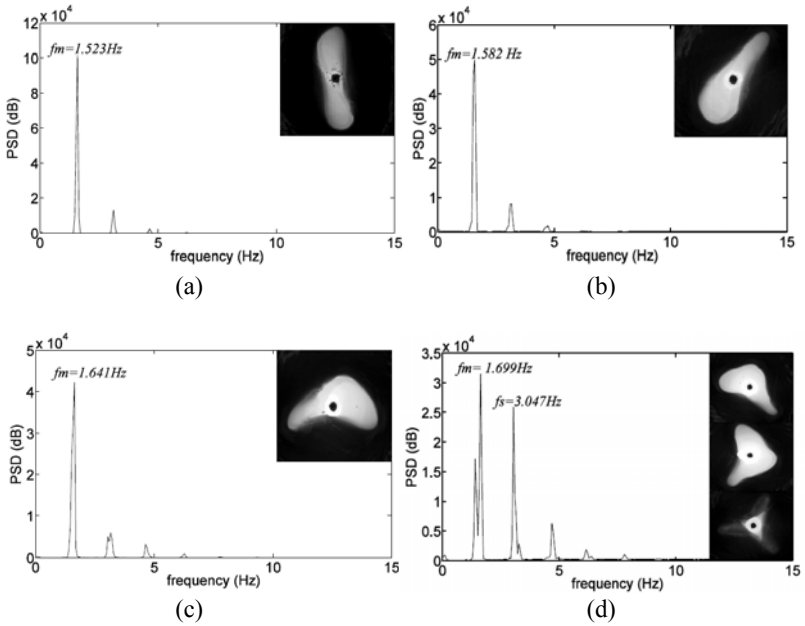

Fig. 4. (a), (b), (c) Oval pattern progression and corresponding Power spectra; and (d) oval to triangular transition $N = 2$ to $N = 3$ and corresponding power spectrum.

3 Results and Discussion

We first discuss results obtained at an initial height h_i = 40 mm where transitions from $N = 2 \rightarrow N = 3$ and $N = 3 \rightarrow N = 4$ were recorded and analyzed using power spectral analysis. Starting with stationary undisturbed flow, the disc speed was set to its starting point of 50 RPM and was then increased with increments of 1 RPM. Sufficient buffer time was allowed after each increment for the flow to equilibrate. At a disc speed of 2.43 Hz the first mode shape (oval) appeared on top of the disc surface. At the beginning of the $N = 2$ equilibrium state, the vortex core is fully flooded. While increasing the disc speed gradually, several sets of 1500 8-bit gray-scale images were captured and recorded. Recorded sets ranged 3 RPM in between. Systematic tracking of the patterns speed and shape evolution were recorded and the recorded images were processed. The evolution of the oval equilibrium state shape and rotating frequency is shown in Figures 4a to 4d. Starting with a flooded core at f_p = 0.762 Hz in figure 4a where the vertex of the inverted bell-like shape free surface barely touched the disc surface, Figure 4b then shows the oval pattern after gaining more centrifugal force by increasing the disc speed by 9 RPM. The core became almost dry and the whole pattern gained more size both longitudinally and transversely with a rotating frequency of f_p = 0.791 Hz. It is

clearly shown that at this instance, one of the two lobes of the pattern became slightly fatter than the other. Figure 4c shows shape development and rotational speed downstream the $N = 2$ range of existence. It is important to mention that once the oval pattern is formed, further increase in the disc speed, therefore the centrifugal force applied on the fluid, curved up the oval pattern and one of the lobes became even much fatter giving it a quasi-triangular shape. Figure 4d features the end of the oval equilibrium pattern in the form of a quasi-triangular pattern and therefore the beginning of the first transition process ($N = 2$ to $N = 3$). The transition process is recorded, processed and the corresponding power spectrum was generated (see Figure 4d). The power spectral analysis revealed two dominant frequencies from the extracted time series function of the captured images; frequency f_m corresponds to the original oval pattern and frequency f_s corresponds to the growing subsequent wave $N = 3$, which is a travelling soliton-like wave superimposed on the original oval pattern therefore forming the quasi-triangular pattern [2]. Further increase of the disc speed resulted in the forming and stabilizing of the triangular mode shape ($N = 3$) with a flooded core; both the troughs and apexes of the polygonal pattern receded and the core area shrank significantly.

Following the same procedure, the development of the triangular pattern and its transition to square ($N = 4$) shape were recorded, image processed and analyzed. Figures 5a to 5e show the power spectra plots and their corresponding sample image from the set recorded and used in generating each of the power spectra. The behaviour of the oval pattern's shape development and transition was also respected for the triangular pattern evolution.

Ait Abderrahmane et al. [2] described the transition process in the form of a rotating solid body N shape associated with a traveling "soliton"-like wave along the vortex core boundary layer. The evidence of such soliton-like wave is revealed here. Figure 6 shows a sample set of colored RGB images during the transition process described above; these images feature the quasi-periodic state during $N = 3$ to $N = 4$ transition described earlier. Giving a closer look at the sequence of images, one could easily figure out the following: the three lobes or apexes of the polygonal pattern are divided into one flatten apex and two almost identical sharper apexes. Keeping in mind that the disc, therefore the polygonal pattern, is rotating in the counter clockwise direction and that the sequence of images is from left to right, by tracking the flatten lobe, one could easily recognize that an interchange between the flatten lobe and the subsequent sharp lobe (ahead) takes place (see third row of images). In other words, now the flattened apex receded to become a sharp stratified apex and the sharp lobe gained a more flattened shape. Such phenomenon visually confirms the fact that transition takes place through a soliton-like wave travelling along the vortex core boundary but with a faster speed than the parent pattern. This first stage of the transition process was referred to as the quasi-periodic stage by Ait Abderrahmane et al. [2]. The quasi-periodic stage takes place in all transitions until the faster travelling soliton-like wave synchronizes with the patterns rotational frequency forming and developing the new higher state of equilibrium pattern. Vatistas et al. [15] found that the synchronization process takes place

when the frequencies ratio of both pattern (N) and the subsequent pattern developed by the superimposed soliton wave ($N+1$) lock at a ratio of $(N-1)/N$. Therefore, for transition from $N = 2$ to $N = 3$, the synchronization takes place when the frequencies ratio is rationalized at 1/2. And the transition $N = 3$ to $N = 4$, takes place when the ratio between both frequencies are equal to 2/3. In the above illustrated two transition processes, the frequency ratio for first transition was equal to $f_N / f_{N+1} = f_m / f_s = 1.69/3.04=0.556 \approx 1/2$. On the other hand, the second transition took place when $f_N / f_{N+1} = f_m / f_s = 3.28/4.92=0.666 \approx 2/3$.

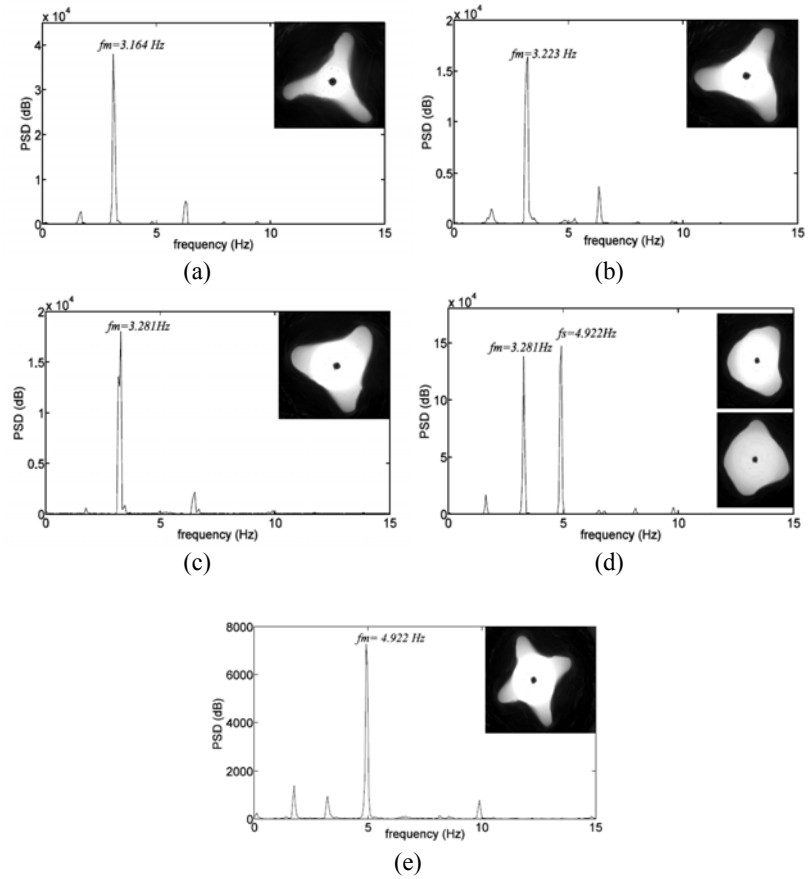

Fig. 5. (a), (b), (c) Triangular pattern progression and corresponding power spectra; (d) Transitional process from triangular to square pattern; and (e) square pattern and corresponding power spectra.

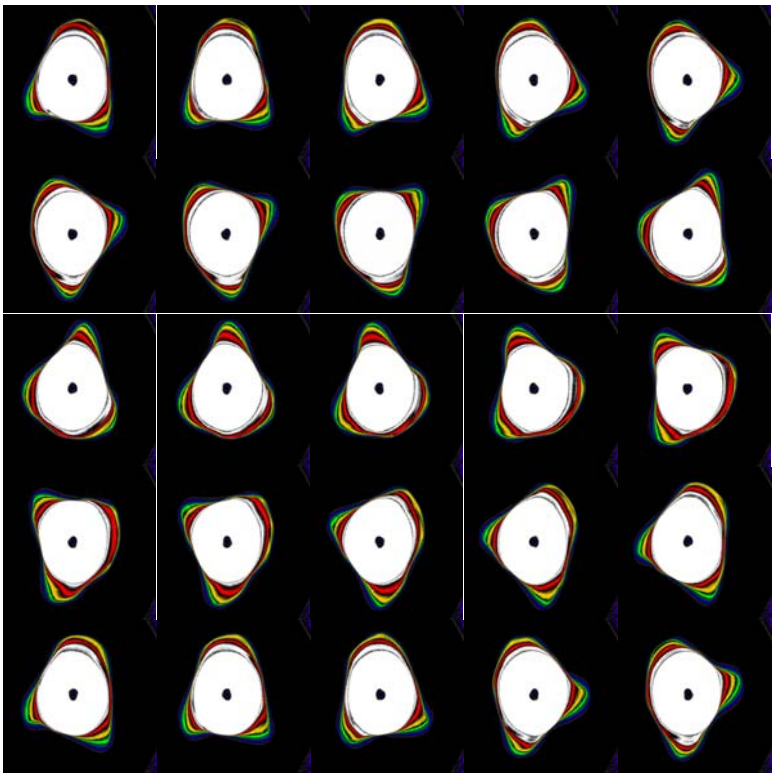

Fig. 6. Quasi-periodic state during triangular to square transition.

Following the same trend, the second experiment was conducted using water at an initial height of 20 mm. At this low aspect ratio, transition between higher mode shapes was tracked and recorded. Using similar setup and experimental procedure, the transition from square mode ($N = 4$) to pentagonal pattern ($N = 5$) and from pentagonal to hexagonal pattern ($N = 6$) were recorded and image-processed for the first time in such analysis. Following the same behavior, the transition occurred at the expected frequency mode-locking ratio. Figure 7a shows the third polygonal transition, from $N = 4$ to $N = 5$. The frequency ratio of the parent pattern to the soliton-like wave is $f_m/f_s = 4.102/5.449 = 0.753 \approx 3/4$. Similarly, Figure 7b shows the transition power spectrum for the last transition process observed between polygonal patterns, which is from $N = 5$ to $N = 6$ polygonal patterns. The frequency ratio $f_m/f_s = 5.625/6.973 = 0.807$ which is almost equal to the expected rational value 4/5. With these two experimental runs, the explanation of the transition process between polygonal patterns observed within hollow vortex core of swirling flows within cylinder containers under shallow water conditions is confirmed for all transitional processes.

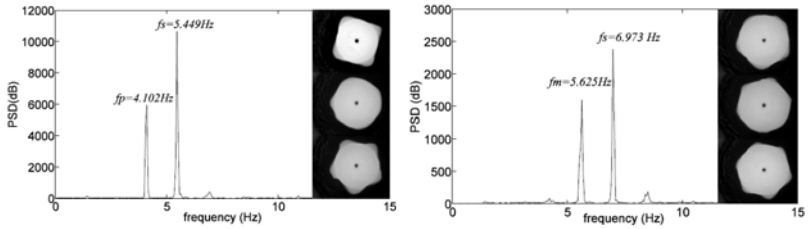

(a) (b)

Fig. 7. (a) Square to pentagonal transition; and (b) pentagonal to hexagonal transition.

Initial height (h_i)		**h_i = 20 mm**			**h_i = 30 mm**			**h_i = 40 mm**	
Transition (*N*) - (*N+1*)		**3 - 4**	**4 - 5**	**5 - 6**	**2 - 3**	**3 - 4**	**4 - 5**	**2 - 3**	**3 - 4**
Viscosity x μ water	**1**	0.697	0.787	0.829	0.545	0.68	0.74	0.558	0.69
		4.6%	4.9%	3.6%	9.0%	2.0%	7.5%	11.6%	3.5%
	2	0.667	0.747	--	0.558	0.671	--	0.557	0.678
		0.1%	0.4%	--	11.6%	0.7%	--	11.4%	1.7%
	4	0.64	--	--	--	0.671		0.557	0.686
		4.0%	--	--	--	0.7%		11.4%	--
	6	--	--	--	--	0.6667		0.55	--
						0.0%		10.0%	
	8					--		0.536	
								7.2%	
	11							0.58	
								16.0%	
	15							0.552	
								10.4%	
	22							0.559	
								11.8%	
fm/fs									
%error									

Table 1. Transition mode-locking frequencies for different liquid viscosities.

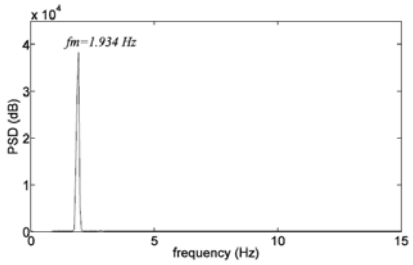

Fig. 8. Power spectrum for $N = 2$ pattern replica

The influence of the liquid viscosity on the transitional process from any N mode shape to a higher $N+1$ mode shape is also investigated. As described earlier, eight different liquid viscosities were used in this study ranging from 1 up to 22 times the viscosity of water. All transitional processes between subsequent mode shapes were recorded, and acquired images were processed. Using the same procedure as in the last section, the frequency ratio of the parent pattern N and the subsequent growing wave $N+1$ has been computed and tabulated in Table 1. As shown in Table 1, the maximum deviation from the expected mode-locking frequency ratio (f_m/f_s) always appeared in the first transition ($N = 2$ to $N = 3$). A reasonable explanation for such induced error is the fact that, the higher the number of apexes per full pattern rotation, the more accurate is the computed speed of the pattern using the image processing technique explained before. Therefore, throughout the conducted analysis, the most accurate pattern's speed is the hexagon and the least accurate is the oval pattern. Apart from that significant deviation, one can confidently confirm that even at relatively higher viscous swirling flows, the transition between polygonal patterns instabilities takes place when the parent pattern (N) frequency and the developing pattern $(N+1)$ frequency lock at a ratio of $(N-1)/N$, Vatistas et al. [15].

As explained earlier, transition has been found to occur in two main stages being the quasi-periodic and the frequency-locking stages [2]. It is also confirmed that frequency mode-locking does exist in polygonal patterns transition irrelative of the mode shapes, liquid heights and the liquid viscosity (within the studied region). In this section, the quasi-periodic phase will be further elucidated and confirmed. Earlier in this paper the quasi-periodic state in the transition of $N = 3$ to $N = 4$, using water as the working fluid, was observably described in Figure 6. To further analyze the quasi-periodic stage, a technique has been developed which animates the actual polygonal patterns instabilities but without the existence of the speculated travelling soliton-like wave along the patterns boundary layer. Using MAPLE plotting program, all mode shapes replica have been plotted and printed. Table 2 shows the plots and their corresponding plotting functions. Printed images were glued to the rotating disc under dry conditions one at a time. The disc was rotated with corresponding pattern's expected speeds under normal working conditions. Such technique

gave full control of the rotating pattern. Therefore, both speed and geometry of the patterns were known at all times. Sets of 1500 8-bit images were captured and processed using similar computing procedure.

N	Pattern plot	Plot function
2	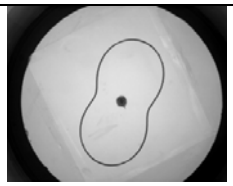	$r = 1 + 0.2 \sin(2\theta)$
2 - 3		$r = 1 + 0.2 \sin(2\theta) + 0.1 \sin(3\theta + 1)$
3	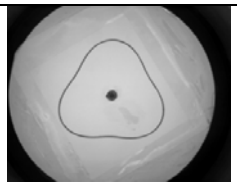	$r = 1 + 0.1 \sin(3\theta)$
3 - 4	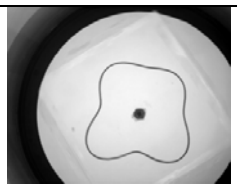	$r = 1 + 0.1 \sin(3\theta) + 0.15 \sin(4\theta + 1)$
4	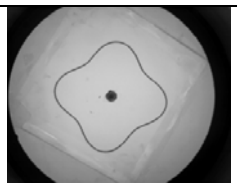	$r = 1 + 0.15 \sin(4\theta)$

Table 2. Patterns replica with corresponding functions.

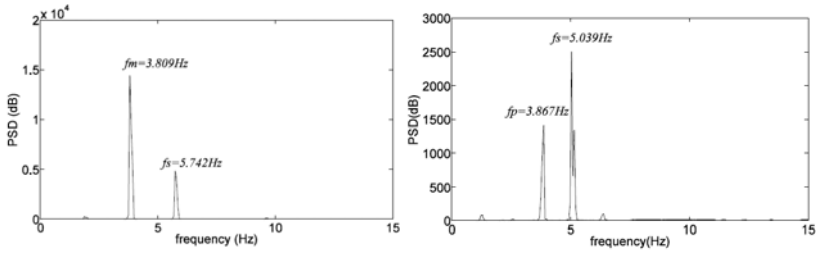

(a) (b)

Fig. 9. Power spectrum of transition processes using patterns replica (a) $N = 2$ to $N = 3$; and (b) $N = 3$ to $N = 4$

Power spectra of the processed sets of images revealed similar frequency plots. Starting with the oval-like shape, the disc was rotated at a constant speed of 1 Hz and the power spectrum was generated from the extracted images and plotted as shown in Figure 8. Since the oval pattern speed is controlled in this case (by disc speed), the frequency extracted could have been presumed to be double the disc frequency (2 Hz). The actual frequency extracted is shown in Figure 8, f_m = 1.934 Hz (3.3% error). Following the same procedure, other polygonal patterns replica were printed to the disc, rotated, captured and processed subsequently. Figures 9a and 9b show the power spectra generated from rotating the quasi-triangular and the quasi-square patterns, respectively.

Figure 9a shows a power spectrum generated from the set of pictures featuring a quasi-triangular pattern captured at 30 fps. The power spectrum revealed two dominant frequencies being f_m = 3.809 Hz and f_s = 5.742 Hz corresponding to the oval and triangular patterns, respectively. Since the quasi-triangular pattern is stationary and under full control, it could have been presumed that the frequency ratio would have a value of 2/3 since the replica pattern is generated by superimposing the oval and triangular functions. The actual extracted frequency was f_m/f_s = 3.81/5.74 = 0.663 ≈ 2/3. Comparing this frequency ratio with the real polygonal patterns mode-locking ratio of 1/2 described earlier, it is clear that the ratio is totally different which proves that both patterns are not behaving equivalently although having generally similar instantaneous geometry. Therefore, the actual rotating pattern does not rotate rigidly as the pattern replica does, but rather deforms in such a way that the ratio of the two frequencies is smaller which confirms the idea of the existence of the fast rotating soliton-like wave (f_s). Moving to the second transition process, triangular to square, as shown in Figure 9b, the frequency ratio was found to be 3/4 as expected since the function used to plot the quasi-square pattern is the superposition of both functions used in plotting the pure triangular and square patterns given in Table 2. Comparing this ratio with the actual mode-locking ratio of 2/3 observed with real polygonal patterns, it is obvious that the ratio is

still smaller which respects the existence of a faster rotating wave along the triangular pattern boundary that eventually develops the subsequent square pattern as visualized earlier using the colored images. From these two experiments, along with the visual inspection discussed earlier, the existence of the fast rotating soliton-like wave (*N+1*) along the parent pattern boundary layer (*N*) is verified, therefore, the quasi-periodic stage.

4 Conclusions

Through the analysis of the present experimental results from different initial conditions, we confirmed with further evidences and generalized the mechanism leading to transition between two subsequent polygonal instabilities waves, observed within the hollow vortex core of shallow rotating flows. The transition follows the universal route of quasi-periodic regime followed by synchronization of the two waves' frequencies. We shows, for the first time, all observed transitions from *N-gon* to a subsequent (*N+1)-gon* occur when the frequencies corresponding to *N* and *N+1* waves lock at a ratio of *(N-1)/N*. The effect of varying the working fluid viscosity on the transitional processes between subsequent polygonal patterns was also addressed in this paper.

Both stages of the transitional process were further explored in this work. The quasi-periodic stage was first tackled using two different techniques, a visual method and an animated method. The deformation of the colored stratified boundary layers of polygonal patterns were inspected during transition process of polygonal patterns and the existence of a fast rotating wave-like deformation was recognized which confirms the idea of the co-existence of a soliton-like wave that initiates the quasi-periodic stage at the beginning of the transition. In order to further materialize this observation, experiments were re-conducted using fixed patterns replica featuring the quasi-periodic geometry of polygonal patterns under dry conditions. Such technique allowed full control of the patterns geometry and speed at all time, therefore working as a reference to the real experiment performed under wet conditions. The experiments revealed an interesting basic idea that was useful when addressing the significant difference in behavior associated with the real patterns transitions. The second part of the transition process included the frequency mode-locking ratio of subsequent patterns. Dealing with the first part of the transition process as being a bi-periodic state or phase, in order for such state to lose its stability, a synchronization event has to occur [4]. This synchronization has been confirmed to occur when the frequency ratio of the parent pattern *N* to the subsequent pattern *N+1* rationalized at *(N-1)/N* value [15]. The frequency mode-locking phenomenon was found to be respected even at relatively higher viscosity fluids when mixing glycerol with water.

Acknowledgment

This work is supported by the Natural Sciences and Engineering Research Council of Canada (NSERC)

References

1. H. Ait Abderrahmane. *Two Cases of Symmetry Breaking of Free Surface Flows.* Ph.D. Thesis, Concordia University, Montreal, Canada, 2008.
2. H. Ait Abderrahmane, M.H.K. Siddiqui and G.H. Vatistas. Transition between Kelvin's equilibria. *Phys. Rev. E* 80, 066305, 2009.
3. H. Ait Abderrahmane, K. Siddiqui, G.H. Vatistas, M. Fayed and H.D. Ng. Symmetrization of polygonal hollow-core vortex through beat-wave resonance. *Phys. Rev. E* 83, 056319, 2011.
4. P. Bergé, Y. Pomeau and C. Vidal. *Order Within Chaos* Hermann, Paris, 1984.
5. J.M. Chomaz, M. Rabaud, C. Basdevant and Y. Couder. Experimental and numerical investigation of a forced circular shear layer *J. Fluid Mech.* 187:115-140, 1988.
6. Dow Chemical Company (1995-2010).
7. M.P. Escudier. Observations of the flow produced in a cylindrical container by a rotating endwall. *Experiments in Fluids* 2:189-196, 1984.
8. R.C. Gonzalez, R.E. Woods and S.L. Eddins. *Digital Image Processing Using MATLAB* 7th edition. Prentice Hall, 2004.
9. R. Hide and C.W. Titman. Detached shear layers in a rotating fluid *J. Fluid Mech.* 29:39-60, 1967.
10. T.R.N. Jansson, M.P. Haspang, K.H. Jensen, P. Hersen and T. Bohr. Polygons on a rotating fluid surface *Phys. Rev. Lett.* 96: 174502, 2006.
11. H. Niño and N. Misawa. An experimental and theoretical study of barotropic instability *J. Atmospheric Sciences* 41:1992-2011, 1984.
12. S. Poncet and M.P. Chauve. Shear-layer instability in a rotating system *J. Flow Visualization and Image Processing* 14:85-105, 2007.
13. M. Rabaud and Y. Couder. Instability of an annular shear layer. *J. Fluid Mech.* 136:291–319, 1983.
14. G.H. Vatistas. A note on liquid vortex sloshing and Kelvin's equilibria *J. Fluid Mech.* 217:241-248, 1990.
15. G.H. Vatistas, H. Ait Abderrahmane and M.H.K. Siddiqui. Experimental confirmation of Kelvin's equilibria *Phys. Rev. Lett.* 100, 174503, 2008.
16. H.U. Vogel. *Experimentelle Ergebnisse über die laminare Strömung in einem zylindrischen Gehäuse mit darin rotierender Scheibe* MPI für Strömungsforschung Bericht 6, 1968.